Electronic Supplementary Information

Calcination of WS_3 at different temperatures

WS_3 was calcined at different temperatures to produce WS_2. Fig. S1 shows the complete XRD of the calcined products. From the figure, one can observe that with increasing calcination temperature, the (002) reflections became more crystalline and resolved. At 850°C, we have found the best crystalline WS_2 as seen from the intensity of (002) reflection. We also observe a slight impurity of orthorhombic WO_3 at calcining temperatures 550°C, 650°C and 850°C as shown in Fig.S1. When the temperature is increased to 950°C, the (002) reflections broaden and become less intense along with a higher intensity peak of WO_3. The WS_2 material at 850°C was used for electrochemical characterization based on its purity (< 1wt% WO_3 phase) and crystallinity.

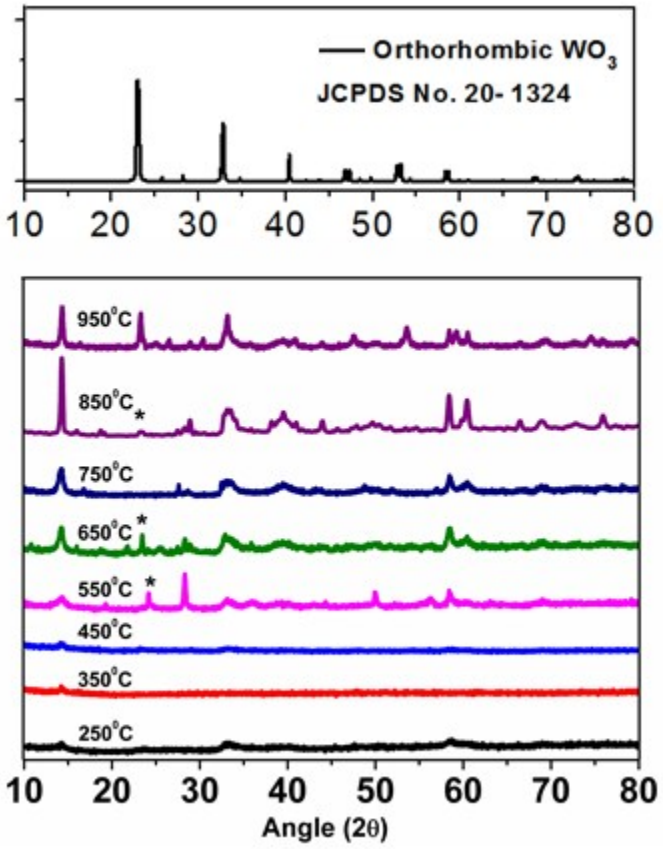

Figure S1. PXRD of WS_3 calcined at different temperatures

FESEM images of WS_2 electrodes before and after cycling

FESEM images of the electrodes were recorded with JSM-7610F, JEOL, Japan, with an accelerating voltage of 20 kV. The electrode images before and after 20 cycles are shown in Fig. S2. The morphology of WS_2 has changed due to repeated insertion/conversion reactions during charging and discharging. The WS_2 platelets/sheets and the acetylene black (AB) added as a conducting agent in the electrode are marked.

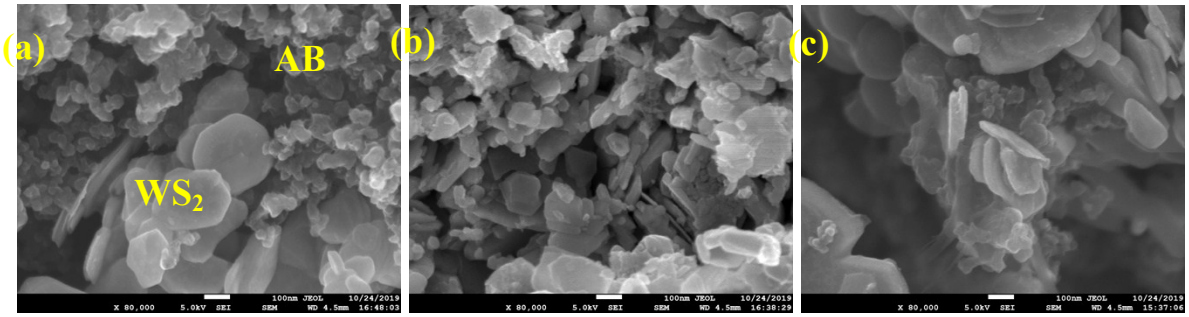

Figure S2. FESEM of the WS_2 electrode (a) pristine (b) after 20 cycles in LIB and (c) after 20 cycles in NIB.

Electrochemical performance of calcined materials

The calcined materials at different temperatures, namely, WS_2 synthesized at 650°C (denoted as WS_2-650), 750°C (denoted as WS_2-750) and 850°C (denoted as WS_2-850) were tested as anodes for both LIB's and NIB's. The charge-discharge curves for the 1st, 2nd and 20th cycles are shown in Fig. S3 (a) to (f). Table S1 shows the reversible capacities obtained after cycle 1 and 20 of all the three samples in LIB and NIB.

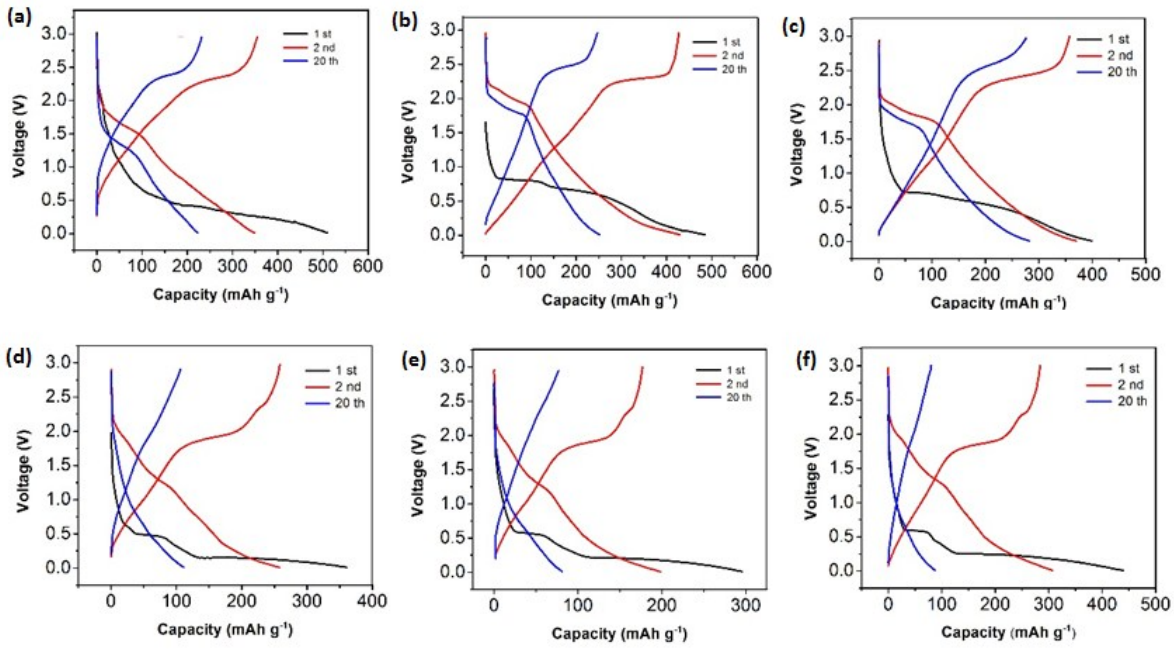

Figure S3. Battery cycling performance of (a) WS_2-650, (b)WS_2-750, (c) WS_2-850 in LIB and (d) WS_2-650, (e)WS_2-750 and (f) WS_2-850 in NIB.

System	Compound	Reversible capacity Cycle 1 (mAh g^{-1})	Reversible capacity Cycle 20 (mAh g^{-1})
Li ion battery	WS_2-650	338.27	216.96
	WS_2-750	479.80	241.45
	WS_2-850	358.50	281.02
Na ion battery	WS_2-650	259.15	110.39
	WS_2-750	176.93	72.79
	WS_2-850	366.36	75.83

Table S1. Reversible capacities obtained after the first and twentieth cycles of WS_2 650, WS_2 750 and WS_2 850 in LIB and NIB.

Synthesis of WS_2/C nanosheets

Citric acid (99 wt%, Loba Chemie) is used as the carbon precursor to synthesize WS_2/C composite. The desired stoichiometric amount of citric acid (8 wt% of C) is added into a beaker with ethanol (99.9%) as the solvent. After complete dissolution under sonication, WS_2 powder was dispersed into this solution at a concentration of 20 mg mL^{-1} and sonicated again for 3h. The solution is filtered, washed, and dried in an oven at 80°C. The powder was carbonized in a tube furnace at

450°C for 1h at a heating rate of 4°C/min under Ar (99.999%). The obtained WS_2/C is characterized using CHNS analysis and powder XRD. PXRD shows phase pure WS_2 after carbonization treatment (Fig. S6). The final carbon wt% in WS_2 from CHNS analysis was found to be 3.84%. Fig. S8 shows the FESEM images of (a) pristine WS_2 nanosheets and (b) carbon-coated WS_2 /C nanosheets.

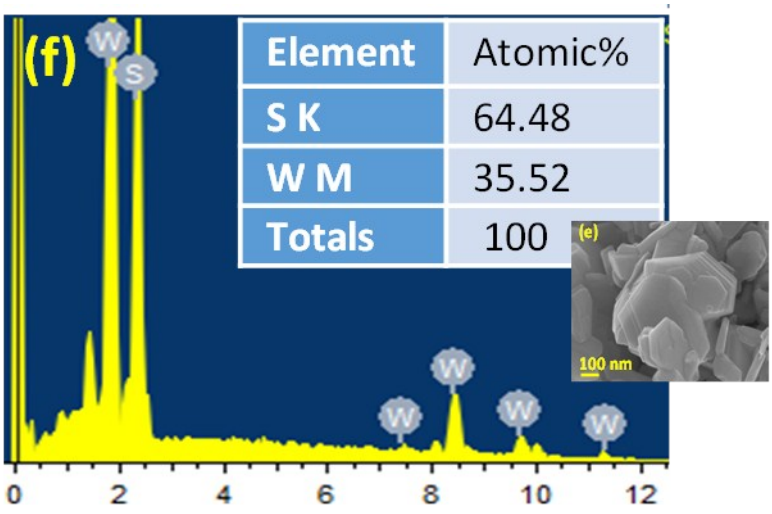

Figure S4. EDX analysis of pristine WS_2 nanosheets.

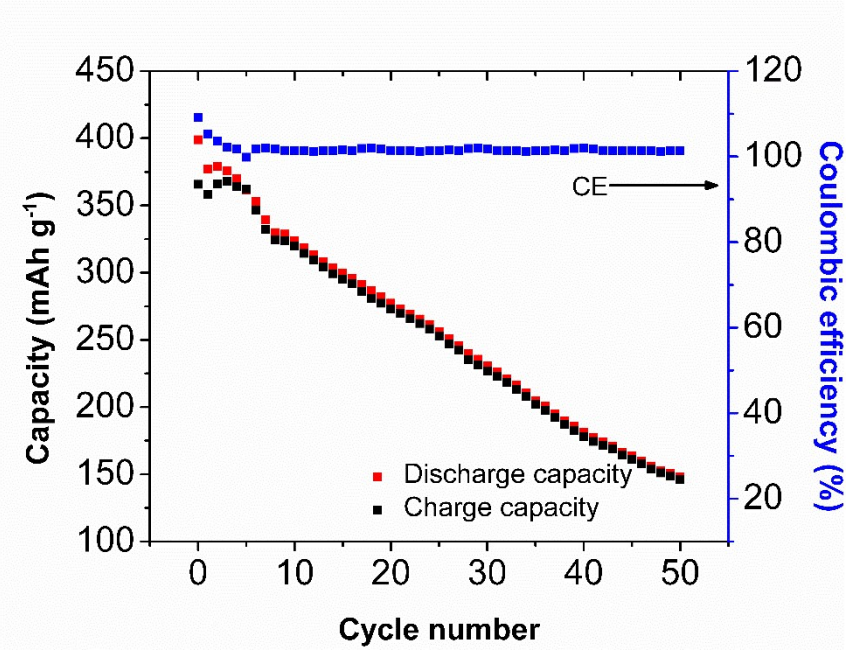

Figure S5. Charge-discharge cycles and CE of pristine WS_2 (*vs. Li/Li*$^+$) at 1C in the voltage range 0.01 V – 3.0 V for 50 cycles.

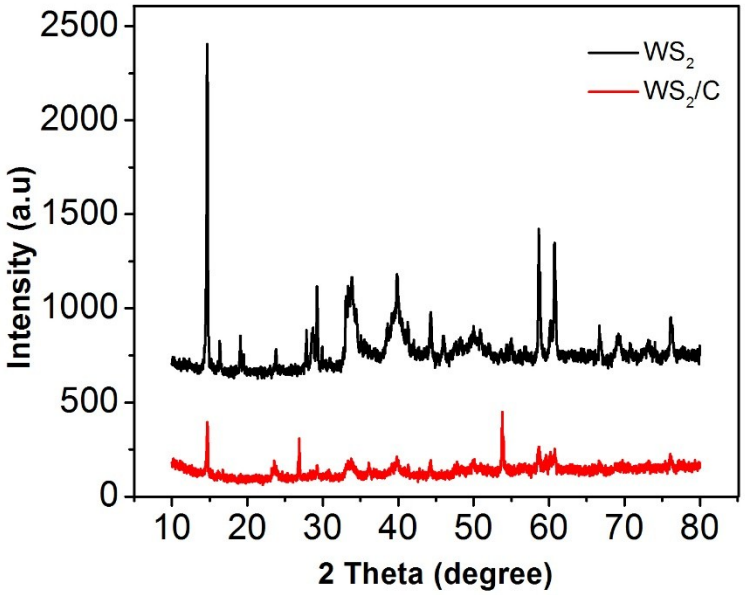

Figure S6. The PXRD of pristine WS_2 and WS_2/C.

Material morphology	C-rate	Sp. Capacity ($mAhg^{-1}$)/Cycle number	References
WS_2- rGO/SWCNT	2.5C	688/1000	1
WS_2/CNF	1C	545/800	2
WS_2/NF/rGO	2.5C	250/200	3
WS_2 /NT/graphene	2.5C	320/500	4
WS_2-double shell C-coating	1C	486/200	5
WS_2-triple shell C-coating	2.5C	784/1000	6
WS_2/C nanosheets	1C	400/700	This work

Table S2. The capacity retention of WS_2@C reported until now at a rate 1C or more and the synthesized WS_2/C nanosheets cycled at 1C rate without any electrolyte additives (FEC, VC).

Raman spectroscopy

Figure S7(a) shows the Raman spectra of WS_2 nanosheets with an excitation wavelength of 514.5 nm. The Raman spectra at $\lambda_{excitation}$ = 514.5 nm shows additional second-order peaks, especially when the number of WS_2 layers in the sample is less than three. The first-order optical modes show the two most prominent peaks seen at 347 cm^{-1} and 416 cm^{-1} correspond to the E^1_{2g} and A_{1g} modes

of vibration. The second-order peaks are observed at 340 cm^{-1} and 321 cm^{-1}. We performed multi-peak Lorentzian fitting on the spectra to deconvolute the observed peaks. The peak at 340 cm^{-1} represents the 2LA (M) mode of vibration. In order to figure out the number of layers in the WS2 sample, we compared the intensity ratio of the peaks. The ratio of peak intensities of E^1_{2g} and A_{1g} modes ($I_{E^1_{2g}}/ I_{A_{1g}}$) is around 0.69, and that of 2LA (M) and A_{1g} ($I_{2LA\ (M)}/ I_{A_{1g}}$) modes is 0.51. Comparing with the reported values, the number of layers of WS_2 present in the nanosheets is more than three.[7] The difference between the peak positions of E^1_{2g} and A_{1g} modes is 69 cm^{-1}, also confirms the presence of more than three layers of WS_2.[8, 9] The AFM height profile (Figure S7 (c)) shows the thickness is approximately 6 nm, which corresponds to the presence of 5-6 layers of WS_2, reaffirming the results of Raman spectroscopy.

Atomic Force Microscopy studies on pristine WS_2

Synthesized WS_2 nanosheets were characterized by AFM. Fig. S7 (b) and (c) show the AFM image and the particle thickness distribution, respectively. Particle thickness was found to be approximately 6 nm, considering a substrate roughness of 4 nm. This value matches well with the crystallite size value of 7.1 nm obtained from the XRD data.[7, 12, 13]

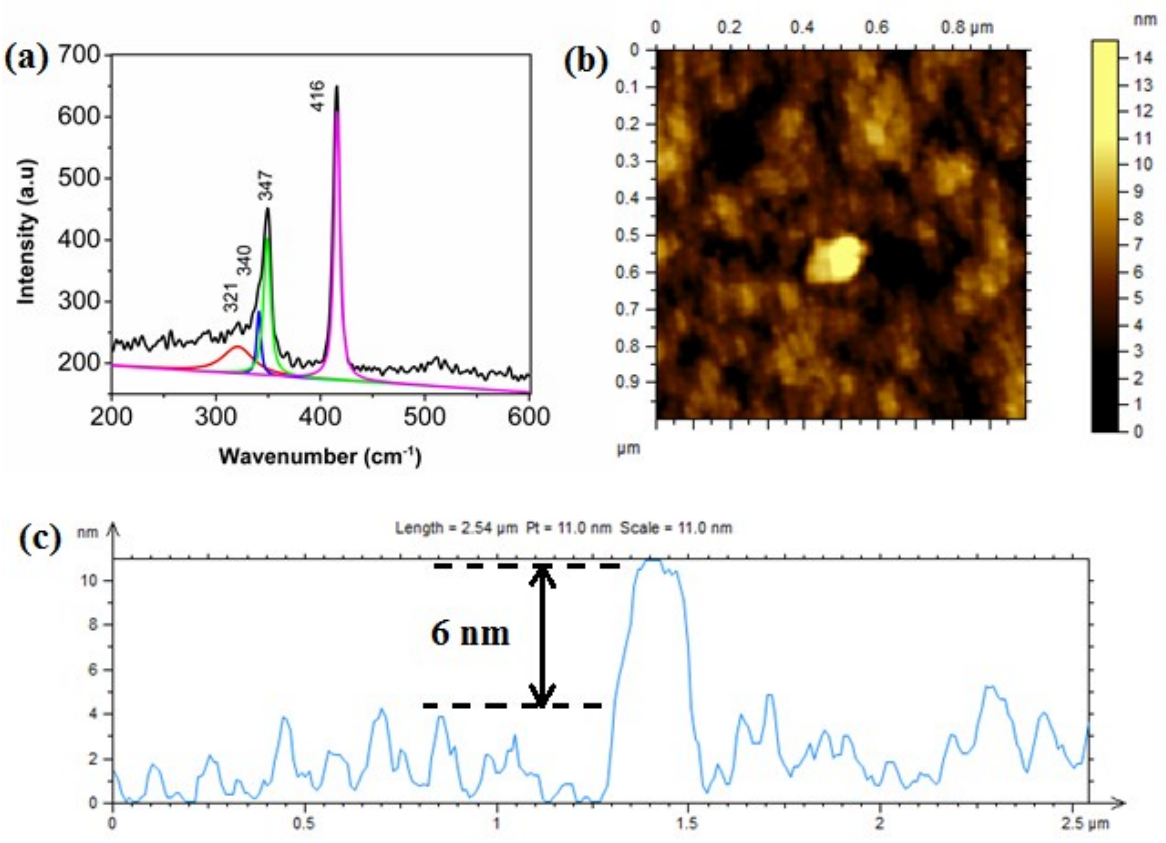

Figure S7. (a) Raman spectra of WS_2 nanosheets with 514.5 nm laser excitation along with multi-peak Lorentzian fitting. (b) AFM of WS_2 nanosheets and (c) particle thickness distribution

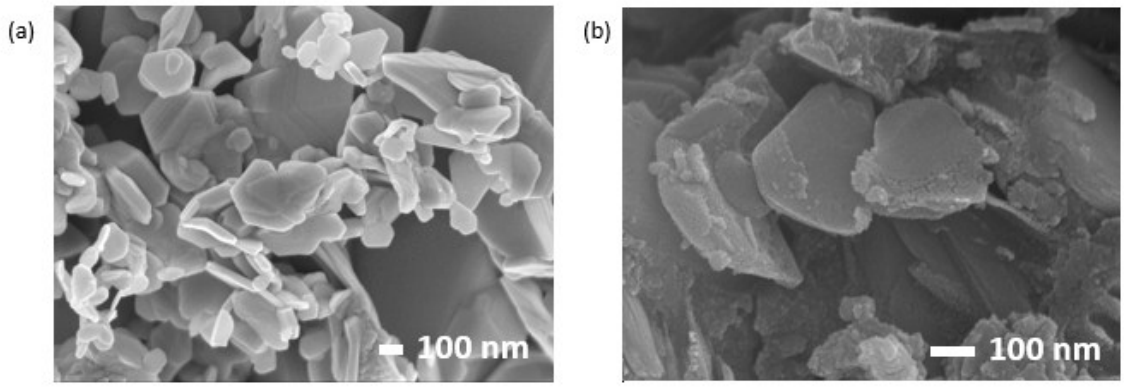

Figure S8. FESEM images of (a) pristine WS_2 nanosheets (b) carbon coated WS_2 /C nanosheets

Electrochemical Impedance Spectroscopy measurements

EIS measurements were carried out on pristine WS_2 and WS_2/C electrodes in LIB and NIB. The Nyquist plots obtained are shown in Fig. S9 (a) to (e). The circuit is shown in Fig. S9 (a) was used to fit the EIS data for pristine WS_2 in LIB and NIB. The amorphous carbon in WS_2/C composite, shows a capacitive effect during cycling. This changes the overall interface behavior of the material during cycling. So, for WS_2/C electrode, the circuit in Fig. S10(a) was used for fitting the before cycling data and Fig. S10 (b) for after cycling data. R_S, R_{CT} and R_{SEI} refer to the resistances of the solution, charge transfer resistance at the interface and the SEI layer resistance respectively. Q1 and Q2 are the constant phase elements associated. W1 refers to the Warburg impedance related to ion diffusion in the bulk of WS_2. EIS was carried out on the cells in the frequency range 10 kHz to 10 mHz before and after cycling them for 20 cycles each at 1C rate from 0.01V – 3.0V.

Fig. S9 (a), (b) and (c) show the Nyquist plots of the impedance of WS_2 battery in LIB and NIB and that of WS_2/C in LIB. From all the three graphs, it is clearly seen that the diameter of the semicircle is reducing after cycling, which indicates the charge transfer (CT) resistance is decreasing. Table S3 shows fitting results obtained from EIS data and confirms the improving CT kinetics with cycling.

During the first discharge process, conversion reaction happens to lead to the formation of metallic tungsten and Li_2S in the case of LIB and metallic W and Na_2S in the case of NIB. This improves conductivity, thereby reducing the impedance after 20 cycles.[10] R_{SEI} increases indicating formation and thickening of the SEI after the first cycle.[2,14-16]

Fig. S9 (d) and (e) show the EIS plots of WS_2 pristine and WS_2/C in LIB. The impedance of WS_2/C is much lower than that of the pristine, showing a better CT kinetics from the improved electrical conductivity of the WS_2/C composite sample.

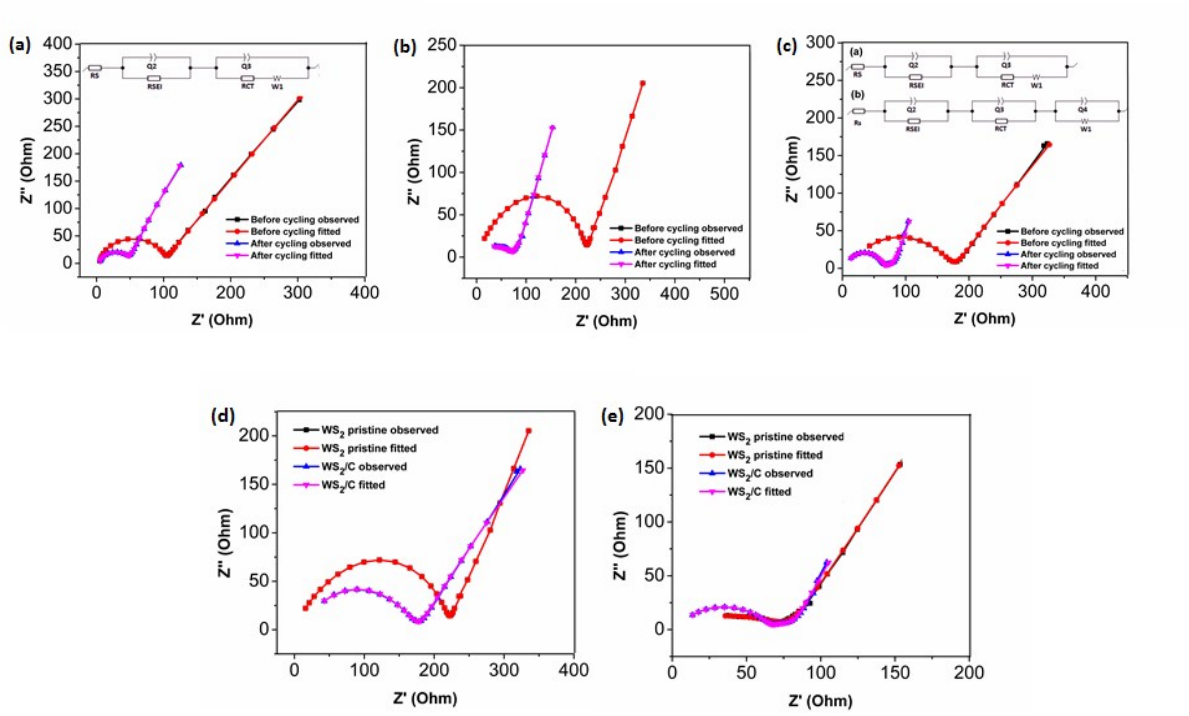

Figure S9. EIS of (a) WS_2 pristine with Na (b) WS_2 pristine with Li (c)WS_2/C with Li (d) comparison of WS_2 pristine and WS_2/C with Li before cycling (e) after cycling.

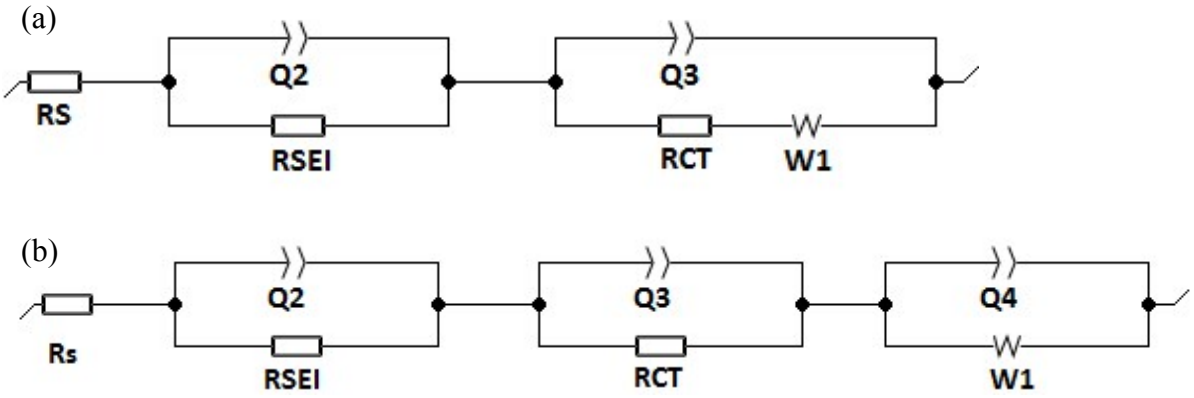

Figure S10: Equivalent circuits (EC) used for fitting the EIS data (a) was used for fitting the EIS data of pristine WS_2 in LIB and NIB. For WS_2/C (a) was used to fit before cycling data and circuit (b) for after cycling data.

S. No.	Compound	R_S (Ohm)		R_{SEI} (Ohm)		R_{CT} (Ohm)	
		Before	After 20 cycles	Before	After 20 cycles	Before	After 20 cycles
1.	WS_2 with Na	1.688	1.795	1.566	4.259	90.65	47.17
2.	WS_2 with Li	2.483	13.44	11.6	14.51	227.1	96.61
3.	WS_2/C with Li	2.451	2.947	15.2	15.39	185.4	63.04

Table S3: Fitting results obtained from EIS data in Fig.S9.

References for SI

1 J. Ren, Z. Wang, F. Yang, R. Ren and Y. Lv, *Electrochim. Acta*, 2018, 267, 133–140.

2 C. Wu, X. Zeng, P. He, L. Chen and W. Wei, *Adv. Mater. Interfaces*, 2018, 5, 1701080, 1–8.

3 S. Liu, B. Shen, Y. Niu and M. Xu, *J. Colloid Interface Sci.*, 2017, 488, 20–25.

4 R. Chen, T. Zhao, W. Wu, F. Wu, L. Li, J. Qian, R. Xu and H. Wu, *Nano Lett.* 2014, 14, 5899−5904.

5 Y. Du, X. Zhu, L. Si, Y. Li, X. Zhou and J. Bao, *J. Phys. Chem. C*, 2015, 119, 28, 15874-15881.

6 X. Zhang, R. Zhao, Q. Wu, W. Li, C. Shen, L. Ni, H. Yan, G. Diao and M. Chen, *J. Mater. Chem. A*, 2018, 6,19004–19012.

7 A. Berkdemir, H. R. Gutiérrez, A. R. Botello-Méndez, N. Perea-López, A. L. Elías, C. I. Chia, B. Wang, V. H. Crespi, F. López-Urías, J. C. Charlier, H. Terrones and M. Terrones, *Sci. Rep.*, 2013, **3**, 1–8.

8 F. Wang, I. A. Kinloch, D. Wolverson, R. Tenne, A. Zak, E. O'Connell, U. Bangert and R. J. Young, *2D Mater.*,2016, **4**, 015007.

9 L. Yuan and L. Huang, *Nanoscale*, 2015, **7**, 7402–7408.

10 H. R. Gutiérrez, N. Perea-López, A. L. Elías, A. Berkdemir, B. Wang, R. Lv, F. López-Urías, V. H. Crespi, H. Terrones and M. Terrones, *Nano Lett.*, 2013, **13**, 3447–3454.

11 M. Sahu, L. Narashimhan, O. Prakash and A. M. Raichur, *ACS Appl. Mater. Interfaces*, 2017, **9**, 14347–14357.

12 M. Chhowalla, H. S. Shin, G. Eda, L.-J. Li, K. P. Loh and H. Zhang, *Nat. Chem.*, 2013, **5**, 263–75.

13 W. Yang, J. Wang, C. Si, Z. Peng, J. Frenzel, G. Eggeler and Z. Zhang, *J. Mater. Chem. A*, 2015, **3**, 17811–17819.

14 Y. Von Lim, Y. Wang, D. Kong, L. Guo, J. I. Wong, L. K. Ang and H. Y. Yang, *J. Mater.*

Chem. A, 2017, **5**, 10406–10415.

15 X. Wang, J. Huang, J. Li, L. Cao, W. Hao, Z. Xu and Q. Kang, *Electrochim. Acta*, 2016, **222**, 1724–1732.

16 M. C. Liu, H. Zhang, Y. X. Hu, C. Lu, J. Li, Y. G. Xu and L. Bin Kong, *Sustain. Energy Fuels*, 2019, **3**, 1239–1247.